Article:
Deng, Y. orcid.org/0000-0002-8804-9428, Xie, N., Hu, W. orcid.org/0000-0003-0254-8363 et al. (17 more authors) (2023) Atomic plane misorientation assisted crystalline quality improvement in epitaxial growth of AlN on a nanopatterned sapphire (0001) surface for deep ultraviolet photoelectric devices. ACS Applied Nano Materials, 6 (6). pp. 4262-4270. ISSN 2574-0970

https://doi.org/10.1021/acsanm.2c05372

Atomic Plane Misorientation assisted crystalline Quality Improvement in epitaxial Growth of AlN on nano-patterned Sapphire (0001) Surface for Deep Ultraviolet Photoelectric Devices

Yong Deng[#1,2], Nan Xie[#,3,4], Wenyu Hu[5], Zhenyu Ma[1], Fujun Xu[4], Longqing Chen[6], Wenbin Qiu[6], Lin Zhao[1], Hong Tao[1], Bo Wu[1], Yi Huang[1], Jian Ma[1], Xiaoyi Wang*[,1,7,8], Xuqi Zhang[1], Yang Qiu*[,2], Xudong Cui*[,7], Chaoyuan Jin[8,9,10], Marie-Pierre Chauvat[11], Pierre Ruterana[11], Thomas Walther[12]

Affiliations

[1]College of Electronic and Information, Southwest Minzu University, State Ethnic Affairs Commission, Chengdu 610047, China

[2]Pico center, SUSTech Core Research Facilities, Southern University of Science and Technology, Shenzhen 518055, China

[3]Institute of Integrated Circuits, China Center for Information Industry Development, Beijing 100048, China

[4]State Key Laboratory of Artificial Microstructure and Mesoscopic Physics, School of Physics, Peking University, Beijing 100871, China

[5]Department of Physics, Southern University of Science and Technology, Shenzhen 518056, China

[6]Key laboratory of Radiation Physics and Technology of Ministry of Education, Institute of Nuclear Science and Technology, Sichuan University, Chengdu 610064, China

[7]Institute of Chemical Materials, China Academy of Engineering Physics, Mianyang 621900, China

[8]Institute of Microelectronics and Nanoelectronics, College of Information Science and Electronic Engineering, Zhejiang University, Hangzhou 310007, China

[9]Zhejiang Laboratory, Hangzhou 311121, China

[10]International Joint Innovation Center, Zhejiang University, Haining 314400, China

[11]CIMAP, UMR 6252, CNRS-ENSICAEN-CEA-UCBN, 6 Boulevard Maréchal Juin, 14050 Caen, Cedex 04, France

[12]Dept. Electronic & Electrical Eng., University of Sheffield, Mappin St., Sheffield S1 3JD, UK

*Authors to whom correspondence should be addressed: 80300024@swun.edu.cn, qiuy@sustech.edu.cn, xudcui@caep.cn

Abstract

The atomic layer misorientation during the growth of a 5 μm thick AlN thin film on a patterned (0001) sapphire substrate was investigated by the scan rotation approach in a probe aberration corrected scanning transmission electron microscope at nanometer scale. Through the geometrical phase analysis of the resulting twisted atomic structure at different depths below the top surface, it is shown that over 10% of local tensile and compressive strain is balanced in a 1.6° twist of the *c*-planes within the first micron of AlN growth. As a consequence, the formation of threading dislocations is reduced. The in-plane twist is seen to decrease towards the layer surface down to 0.5°. Finally, growth has adopted the conventional step flow mechanism with a reduced density of emerging dislocations by the thickness of 5 μm. Our finding forecasts the possibility of understanding the relationship between atomic bilayer twist and local strain accommodation at nanometer scale, which could provide guidance for achieving better crystal quality of AlN thin films on patterned substrates during epitaxy.

Keywords: *Strain relaxation, strain accommodation, moiré fringes, misorientation, scan rotation, scanning transmission electron microscopy*

Introduction

Due to its short emission wavelength (~210 nm)[1–3], aluminum nitride (AlN) has been under extensive research for applications in ultra-violet opto-electronics.[4–8] However, because of the large lattice mismatch between AlN and sapphire (Al_2O_3),

the threading dislocation density (TDD) is expected to be high[9–11], so access to high crystal quality AlN epilayer can still be a challenge in AlN heteroepitaxial growth. Particularly, due to the large in-plane lattice misorientation (~30°) between Al_2O_3 (0001) and AlN (0001)[12,13], *c*-plane twisting may be expected to occur. Since AlN has the highest stacking fault energy among all nitride semiconductors[14,15], screw and mixed type dislocations across the AlN/Al_2O_3 interface could transform into pure edge TDs along the growth direction[11,16,17], leading to the high density of TDs often reported in direct growth of 1–2 μm AlN epilayers on sapphire substrates[18,19]. However, such high density of TDs was not present in recent epitaxial lateral overgrowth (ELOG) of AlN on nano-patterned sapphire substrates (NPSS), even in 4 μm thick layers[8,20–23].

For example, Xu et al[24] and Tang et al[25], obtained a TDD of only ~10^8 cm^{-2} on a hole-type nano patterned substrate, which was one order of magnitude smaller compared with recent progress in direct growth of AlN epilayers on sapphire substrates (~10^9 cm^{-2})[18,19]. The dislocation density reduction in AlN epitaxy on NPSS is attributed to the voids inducing dislocations to bend over and terminate at internal pores[16,21,25,26], so their propagation towards the surface is reduced. This mechanism can lead to a highly textured crystal orientation in the vicinity of the voids. Indeed, many reports show inhomogeneous contrast around such voids in transmission electron microscopy images under two beam conditions[17,21,22], especially for $\boldsymbol{g}=[11\bar{2}0]$[21,26,27], indicating a possible lattice rotation within the basal plane of AlN. Interestingly, these twisted *c*-plane regions have been considered irrelevant to the

propagation of dislocations in recent models of strain accommodation. Therefore, it is vital to explore the relationship between atomic bilayer misorientation and strain relaxation at the nanometer scale. Unfortunately, to simultaneously measure small crystal misorientations and the strain state simultaneously with nanometer spatial resolution is experimentally difficult even in convergent electron beam nano-diffraction.

In this work, we investigate AlN growth on patterned substrates in order to determine the influence of local strain relaxation on the crystalline layer quality. This has been possible using the latest techniques developed in scanning transmission electron microscopes with aberration correction that allow to monitor without drift or distortions the occurrence of fine moiré fringes[28] at the few Ångstroms scale, as a result of interference between the crystal lattice and a fixed scan pattern. The scan rotation method has been proven to be useful in strain measurement[29–31] and defect magnification[32]. Applying this technique in combination with geometrical phase analysis (GPA), we demonstrate that the crystal quality of AlN thin films on patterned substrates benefits from the continuous decrease of the small angle *c*-plane misorientation until a step flow growth mode with low defect density is reached. Our finding pioneers the feasibility of evaluation of local strain distribution in an atomic bilayer twisted lattice at sub-nanometer scale, which is potentially useful for improving the crystal quality in AlN/NPSS epitaxy as well as the understanding of nano-strain dynamics in a locally distorted lattice.

Experimental

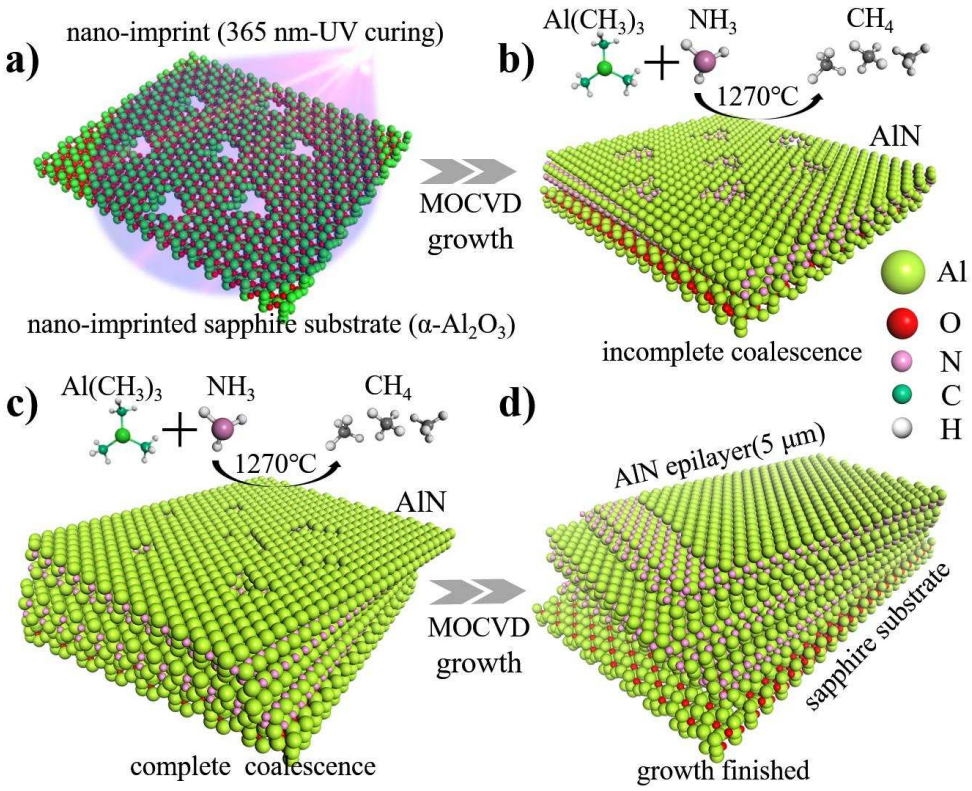

Figure 1. Growth process of AlN epilayer on NPSS a) nano-imprinted sapphire substrate with 365 nm ultraviolet curing, b) incomplete coalescence during AlN growth (epilayer thickness ~1 μm), c) complete coalescence during AlN growth (epilayer thickness ~2.5 μm), d) accomplished epitaxy of AlN (epilayer thickness ~5 μm).

The AlN thin film was grown on Al_2O_3 (0001) pattered by 365 nm wavelength UV light lithography, creating a hexagonal close-packed hole pattern with 1 μm period and approximate 500 nm hole depth to satisfy the principle of small coalescence areas[33]. The epitaxy was carried out in a 3×2" close-coupled showerhead (CCS) Aixtron high-temperature metal-organic chemical vapor phase (MOCVD) system. Trimethylaluminum (TMAl) and NH_3 were used as growth precursors. AlN epilayers

with thickness of 0.5, 1, 2.5 and 5 μm were grown at 1270℃. The process of AlN epitaxy on NPSS is shown in Figure 1, where the details of growth parameters can be found in our previous report[34].

The surface topography at different growth stages was investigated by atomic force microscopy (AFM). A Panalytical RMD X-ray diffractometer (XRD) was used to evaluate the crystal quality of AlN epilayer. In order to investigate the local structure, plan-view and cross-sectional TEM specimens were prepared by focused ion beam (FIB) thinning using a Thermo-Fisher Helios 600i. A 30 kV gallium (Ga) ion beam with a beam current of 0.23–9.3 nA was applied to produce FIB lamella; the specimens were further thinned by a 2 kV Ga ion beam with beam current down to 15 pA. To eliminate the surface oxides, a final surface polishing was carried out in a Fischione Nanomill 1040, where the beam current and accelerating voltage were set as 150 pA and 900 eV respectively. The scan rotation technique and atomic resolution high angle annular dark field (HAADF) imaging were carried out in a Thermo-Fisher Titan Themis G2 double aberration corrected transmission electron microscope at 300kV.

Results and Discussion

To monitor the coalescence procedure, ex-situ AFM investigations at different growth stages were carried out, as seen in Figures 2a–e). At the beginning, triangular shaped holes were observed in Figure 2 a), which indicates incomplete coalescence regions (ICR) in AlN epilayer on NPSS. Then the overgrowth rapidly takes place on the patterned surface covering most of the substrate but still leaving pits at the centers

of the initial triangular holes (Figure 2b). At 1 μm thickness (Figure 2c), the triangular structures have completely disappeared, and the pits exhibit various shapes. When the AlN layer reaches 2.5 μm thickness (Figure 2d), the initial surface morphology has mostly disappeared and the surface is only exhibiting irregularly distributed small triangular defects due to coalescence at pits. Finally, atomic steps are clearly visible at 5 μm thickness demonstrating two-dimensional growth as shown in Figure 2e).

For the epilayer thicknesses up to 2.5 μm, the full width at half maximum (FWHM) of the (0002) diffraction peak of AlN is estimated as ~180 arcsec, which is much narrower than that of the $(10\bar{1}2)$ diffraction peak (~360 arcsec). Since only the TDs with screw components contribute to (0002) peak[16], this is a good indication that pure edge TDs dominate AlN epitaxy before coalescence (Figure 2 d). When the epilayer thickness approaches 5 μm, the (0002) and $(10\bar{1}2)$ X-ray diffraction peaks exhibit FWHM comparable values of 170 and 192 arcsec, respectively (Figure 2g), where the decrease of the $(10\bar{1}2)$ peak width is due to a reduction of edge dislocation density. Therefore, such dislocations in the vicinity of nano-imprinted doles must bend over and disappear at the void facets (Figures 2 h–j).

However, the continuous change of ICR structure observed in AFM (Figures 2a–e) hints at an irregular crystal coalescence leading eventually to high crystal quality of the final AlN epilayer. It is therefore important to reveal the mechanism which governs this coalescence.

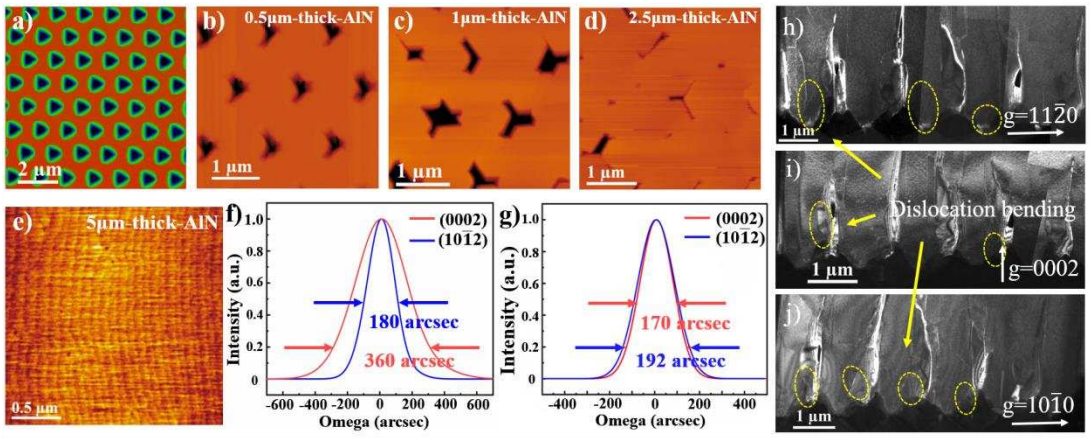

Figure 2. Surface morphology of AlN for epilayer thicknesses of a) 0 µm, b) 0.5µm, c) 1 µm, d) 2.5 µm and e) 5 µm. f) and g) show (0002) and (10$\bar{1}$2) XRD peaks from 2.5 µm and 5 µm AlN thin film. h)–j) display dislocations bending towards the sidewalls of voids.

The bright field overview image of the 5 µm AlN epilayer shows regularly spaced vertical features (Figure 3a) which emanate from the patterned sapphire surface as tubular defects and extend just below the surface, in agreement with the AFM observations (Figure 2e). Between these tubular defects, *a*-type dislocations[35,36] are visible (Figure 3c). The absence of screw or mixed type dislocations in the investigated area and the density of the *a*-type dislocations correlate well with the expectation from XRD results. Inside the field of view of Figures 3b)–d), the vertical defects exhibit an inhomogeneous contrast along the vertical direction. This is probably correlated to changes in the strain due to local orientation variation when the triangular shape of the surface patterns transforms from pits to irregular three-fold openings and finally close up at deposition thicknesses of 5 µm to yield step flow growth on the epilayer surface (Figure 2e).

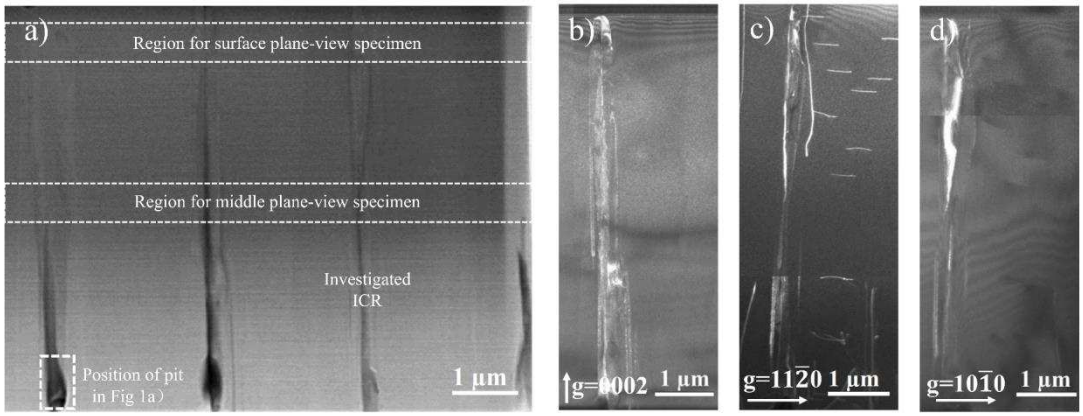

Figure 3. a) Overview of the investigated AlN cross-sectioned 5 µm thick film, b)-d) show weak beam dark field images for incomplete coalescence regions (ICR) with ***g***=0002, 11$\bar{2}$0, 10$\bar{1}$0, respectively.

To appreciate the contribution of any lattice misorientation to the TD density, we carry out a local strain and atomic plane twist analysis. Indeed, any local twist of lattice planes can be determined as it gives rise to moiré fringes in the corresponding images[37]. We take advantage of the high spatial resolution and low geometrical distortion in aberration corrected scanning transmission electron microscopy (AC-STEM) for a direct observation of lattice misorientation induced moiré fringes. The scan rotation technique in scanning transmission electron microscopy (STEM) allows to easily observe moiré patterns at nanometer scale[38], due to the interference of the square scan grid and the hexagonal lattice fringes. The principle of the scan rotation technique is shown in Figure 4.

In a moiré pattern, the interference between two sets of misoriented lattices gives rise to a coarser fringe spacing if the two lattice constants are close enough in length. However, due to the hexagonal lattice coordinates in AlN and square scan grid

coordinates (Figure 4a), their interference might be incompatible with standard Lorentzian formula (SLF) derived for square scan grids and cubic lattices[29]. To reveal the influence of moiré patterns in a space group mismatched system, the relationship between scan rotation angle and extrapolated moiré fringes spacings are compared with the SLF[32] in Figure 4b). It can be seen here that the SLF can be applied to predict the moiré fringe spacing within scan rotation angle ranges from -6° to +6°, where the influence of space group mismatch between hexagonal lattice and square scan grid is negligible under the condition of small scan rotation angle.

To test the angular range within which the SLF model is available for interpreting moiré fringes in strained lattices, a 20 % expansion/compression of the AlN atomic layer was coupled with image plane rotations as shown in the supporting information of Figures S1 and S2. As can be seen in these simulations, within ±6° of scan rotation angle, the moiré fringe spacing agrees with the SLF prediction. Thereby, independent of tensile/compressive strain in AlN, the SLF model is valid for analyzing interference between square scan grid and hexagonal lattices within ±6° of scan rotation angle.

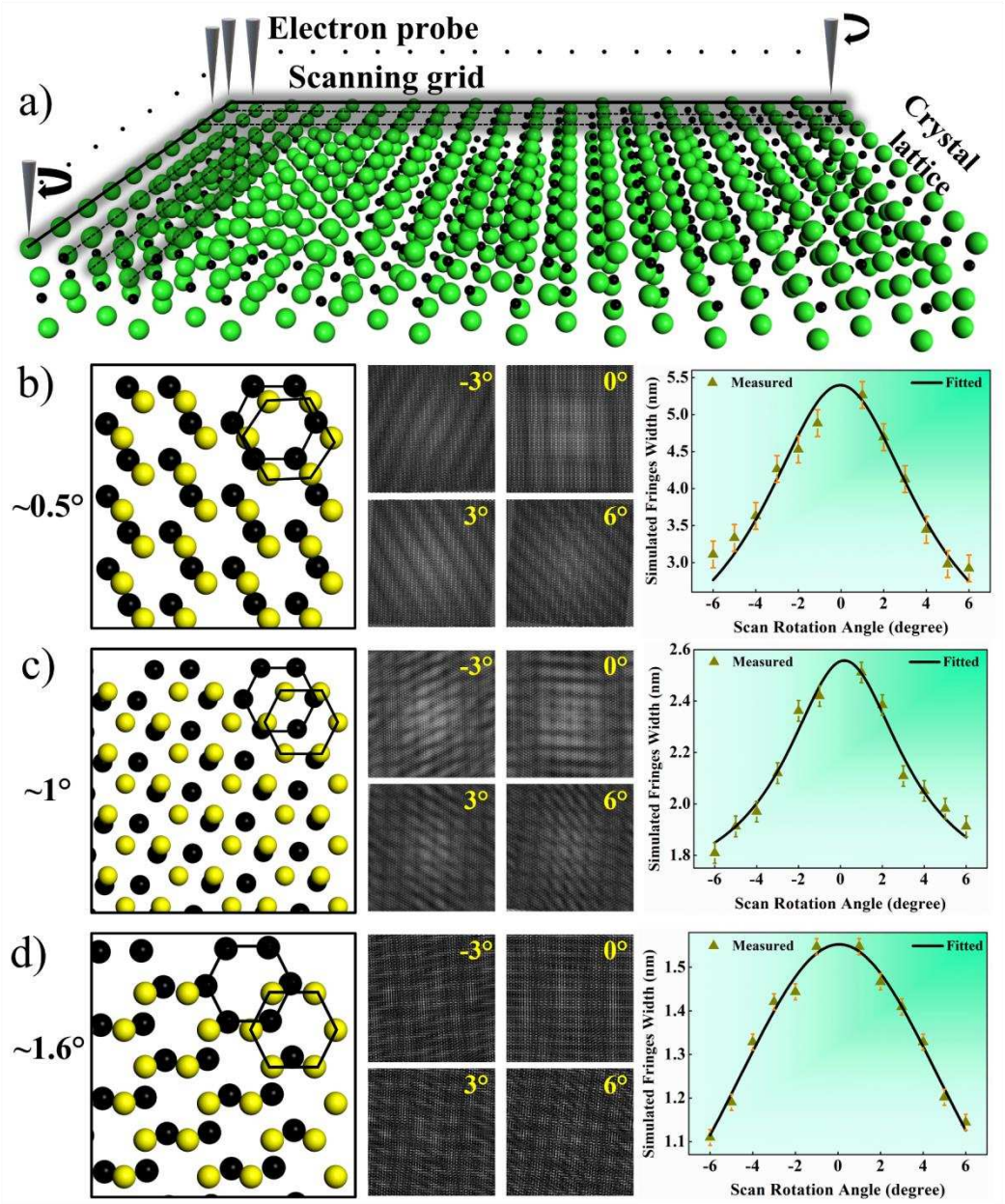

Figure 4. a) Principle of electron beam scanning in STEM. The green and black dots are associated with Al and N atoms respectively, the square scan grid is shown on top of AlN. b)-d) Left column: 0.5°, 1°, 1.6° misoriented AlN structure as well as their in-plane misorientation angle (yellow and black dots represent the upper and lower layers of atomic bilayers). Middle column: the moiré fringes from superimposed hexagonal and square grid. Right column: moiré fringe width as a function of scan rotation angle (-6° to 6°).

In case of atomic bilayer misorientation model, each atomic plane could form its individual moiré patterns with the scan grid pattern, so the superposition of two moiré patterns could restrict the direct implement of SLF model to predict fringe spacings. Therefore, a theoretical model needs to be introduced as a reference for determining *c*-plane twist in scan rotation experiments, In Figure 4 b)–d), three in-plane misoriented AlN atomic bilayers (rotated by twist angles of 0.5º, 1° and 1.6°) in the model were combined with a square scan grid within ±6º of scan rotation angle. All the simulated images show clear periodic moiré fringes, and by measuring the moiré fringe distances for known image plane rotation angles, the lattice rotation of individual *c*-plane twisted models can be recovered from the resulting moiré patterns as shown in Figure 4 b–d). These models were applied as a reference to determine the in-plane lattice misorientation angle.

The scan rotation measurements were then conducted on plane-view specimens extracted from surface and central regions of the 5 µm AlN epilayer. To correlate the experimental with simulation results, the scan rotation angle has been defined as 0° once the maximum spacing of moiré fringes was achieved (Figure 5). The moiré fringes in near-surface area show a strong dependence on scan rotation angle, and the spacing of fringes can vary from ~3.5 nm (Figure 5a) to 5.2 nm (Figure 5b). To determine whether lattice expansion or atomic plane misorientation can describe the observation, the experimental moiré fringes have been compared with theoretical lattice expansion as a function of scan rotation angle (supporting information Figure

S3) and misorientation model (Figure 4). As shown in Figure 5g), ~0.5° lattice misorientation and 2.2% strained lattice describe the experimental observation best.

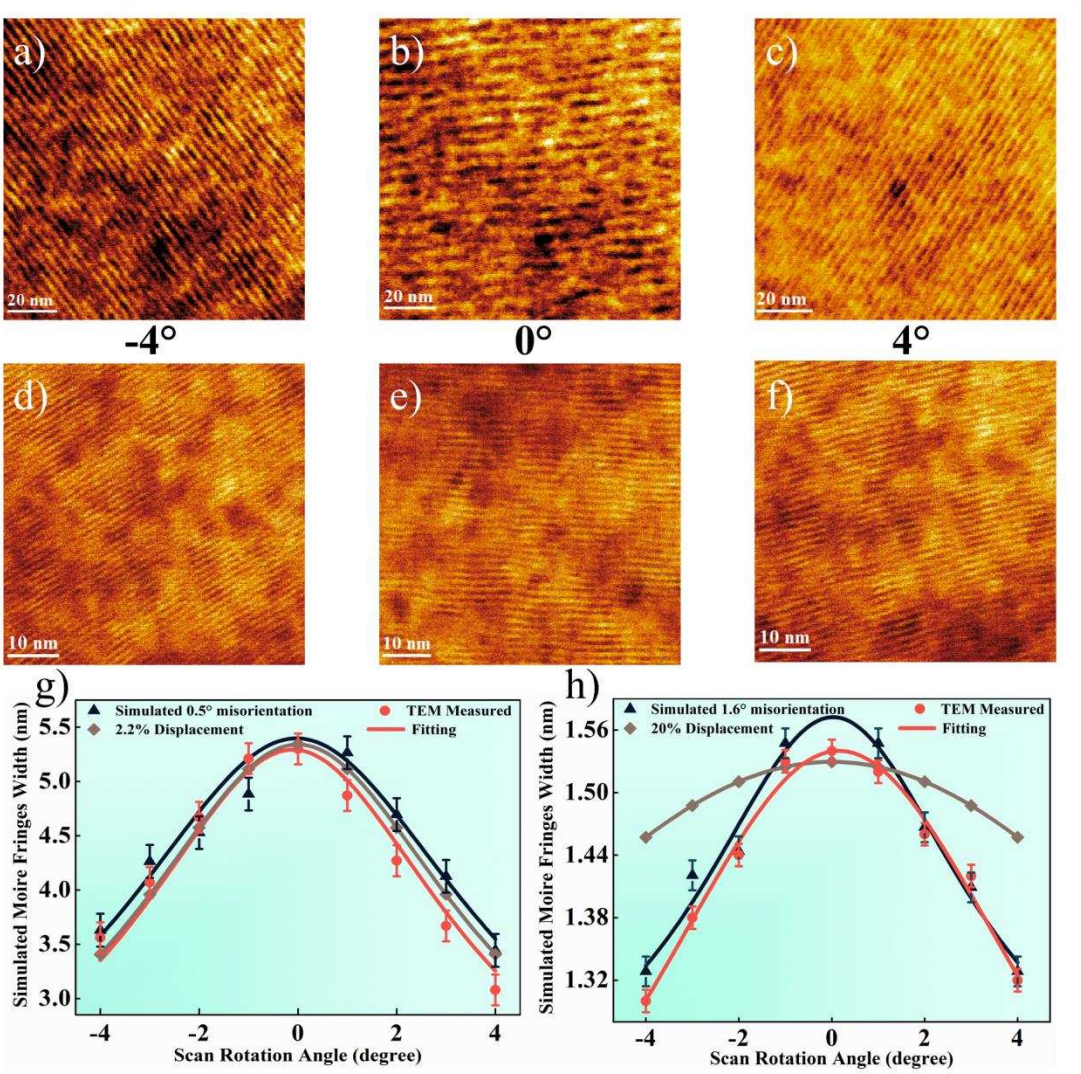

Figure 5. STEM bright field images of moiré fringes of: a)–c) surface region of AlN epilayer; d)–f) middle area of AlN epilayer. Plots of the scan rotation angle as a function of fringe spacing for g) surface region of 5 µm AlN epilayer, and h) central area of 5 µm AlN epilayer, where the red, black and grey curves represent the values from STEM bright field images, misorientation and SLF model respectively.

On the contrary, as can be seen in Figures 5d)–f), in the middle region of the AlN epilayer (~2.5 μm below the surface), a weak dependence of moiré fringe spacings on scan rotation angle is observed. By comparing the experimental and simulated results, none of our lattice expansion SLF models could fully describe the experimental statistics, even for an assumed lattice expansion of 20% (Figure 5 h). Nevertheless, by employing the reference model of lattice misorientation, the results in Figure 5 h) suggest an ~1.6° *c*-plane twist angle. Therefore, the scan rotation technique provides evidence of a gradual decrease of atomic in-plane twist angle along the growth direction, thereby improving the crystal quality of the AlN epilayer.

According to the lattice misorientation angle determined from scan rotation technique, although the maximum twist angle of atomic planes approaches ~1.6°, the in-plane lattice stress failed to further introduce dislocation This could be an indication that there may be strain accommodation in the distorted lattice around the vertical ICR without the contribution from the tilt of AlN sub-grains with respect to sapphire substrate.

To evaluate the contribution from *c*-plane twist in our AlN epilayer, the GPA analysis was first employed to investigate the strain distribution in cross-sectional view of middle and near-surface regions of the epilayer (Figure S6). In Figure S6, a weak strain ε_{zz} in agreement with lattice displacements (LD) < 2% within the (0001) plane was observed in both the near-surface and the middle region of the AlN thin film, which demonstrates a weak *c*-plane twist in the AlN epilayer, which correlates well with observation from XRD and WBDF images. The ε_{xx} strain in the $(01\bar{1}0)$

planes and ε_{xz} shear strain in $(01\bar{1}0)$ planes are strong in the middle region compared to the near surface, which reflects an effective release of internal strain at the top of AlN thin film. Therefore, it is necessary to explore the in-plane twist of (0001) atomic layers. By implementing the GPA on plane-view atomic resolution images, the corresponding strain distributions are shown in Figure 6. In Figure 6 a)–d), a weak strain contour (LD <5%) was observed in the near-surface region of the AlN thin film, which confirms the effectively strain relaxation at the surface.

On the contrary, in Figures 6e)–h), the middle region of AlN epilayer exhibits a strong elastic tensor contour (LD>10%) of ε_{xx} (principal component in $(01\bar{1}0)$), ε_{yy} (principal component in $(2\bar{1}\bar{1}0)$) and ε_{xy} (shear component in $(2\bar{1}\bar{1}0)$[38]), which indicates the existence of a high degree of atomic displacements in both principal and shear axes[39]. Here, it is worth pointing out that the field of view contains both tensile (bright area) and compressive (dark area) regions, which gives an average strain value less than 0.6% (supporting information Table S1) in *xx*, *yy* and *xy* strain components, indicating the local strain is almost balanced inside the field of view. Therefore, by correlating the lattice misorientation results from Figures 5g) and h), the ~1.6° twist of *c*-planes is able to balance the internal strain, which reduces the production of TDs.

Considering the three-fold tubular ICRs, their internal edges can serve as regions relaxing the strain by terminating dislocations at inner surfaces. To determine the role of lattice misorientation in strain relaxation, the atomic displacements in the vicinity of ICRs are revealed in Figures 6i)–p). As shown here, near ICRs a large degree of lattice displacement (LD>10%) appears near the cores, which however fluctuates

strongly and may be due to the weak lattice fringe contrast, related to an accommodation of strain in the amorphous region. Furthermore, apart from the ICR region, the average of strain value in crystalline region remains under 0.6% (supporting information in Table S1), revealing an effective strain relaxation towards the core of ICR. The strain induced crystal deformation at the facets of ICR is connected to the inhomogeneous intensity in WBDF images (Figure 3).

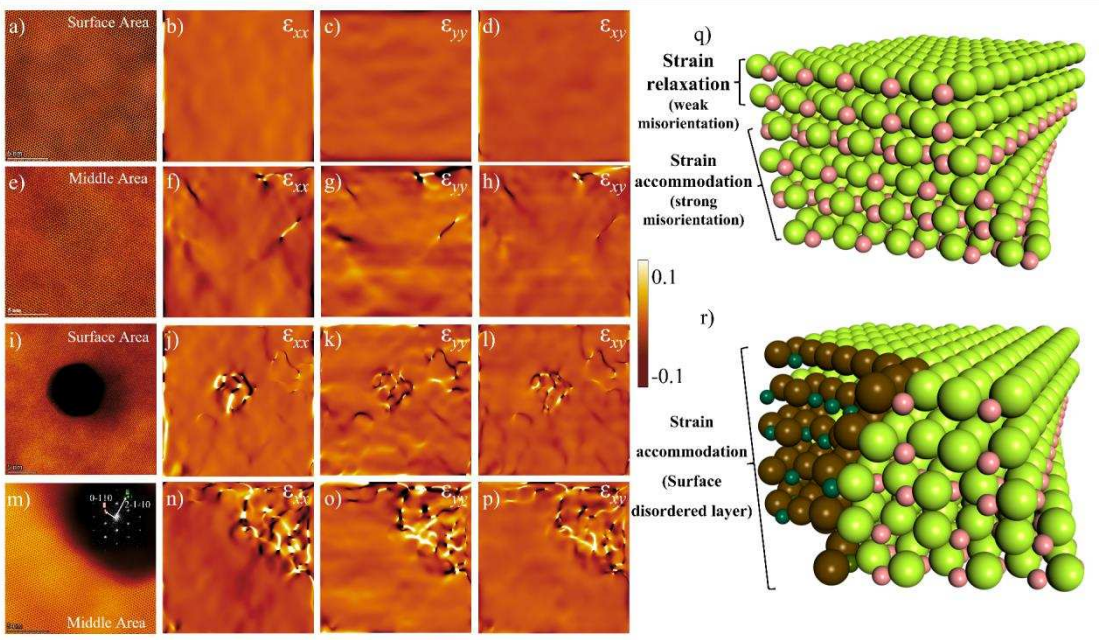

Figure 6. The GPA lattice displacement of a)–d) surface area without ICR, e)–h) middle area without ICR, i)–l) surface area containing ICR core structure, m)–p) region near the core of ICR. Schematic diagrams of AlN crystal growth q) away from ICR and r) near ICR.

Therefore, based on the geometrical phase analysis of the resulting moiré patterns, ignoring the contribution from the small tilts out of the basal planes, two growth modes are proposed in Figures 6q) and r). In the absence of ICR (Figure 6q)), the strain can be accommodated by a strong twist of *c*-planes. As the lattice distortion

gradually decreases towards the surface of the epilayer, the formation of threading dislocations is further suppressed due to the effective relaxation of residual strain. On the contrary, as sketched in Figure 6 r), since the core of ICR relaxes some strain, a relatively low degree of internal strain in the vicinity of ICRs can restrict the formation of TDs. At the top of the layer, almost complete strain relaxation has taken place and the step growth mechanism has taken over, giving rise to the formation of a low dislocation density AlN film with a near-ideal smooth surface.

Conclusion

The lattice misorientation in an AlN epilayer on nano-imprinted substrate was successfully determined by scan rotation induced moiré fringes at the nanometer scale, together with geometrical phase analysis from atomic lattice imaging. At the internal voids produced by the nano-patterning, the dislocations bend and terminate at their internal surfaces instead of propagating to the layer surface. Moreover, the in-plane twist of AlN (0001) planes appears to induce a pronounced lattice displacement, during the coalescence (at ~2.5 μm depth below the growth surface), and a ~1.6° twist of *c*-planes is shown to accommodate over 10% of the internal strain near the ICRs with a balance of local tensile and compressive components being responsible for avoiding the formation of TDs. At the top of the investigated layers (5 μm), the in-plane atomic layer twist angle has gradually reduced to 0.5°. Therefore, the presence of low angle *c*-plane twist appears to be crucial for releasing the atomic layer misorientation induced lattice strain, enabling the growth of high quality AlN thin film on patterned substrates. In summary, this work explains an interesting growth

observation in ELOG of AlN on nano-imprinted sapphire substrates, which could yield general guidance for achieving better crystalline quality layers for optoelectronic applications on mismatched substrates as well as providing a better understanding of nano-strain dynamics in distorted nanocrystals.

Supporting Information

There is supporting information provided, including additional simulations of moiré pattern at various atomic plane twist angles, scan rotation measurements and cross-sectional views with GPA analysis.

Author Information

Corresponding Authors:

Xiaoyi Wang - College of Electronic and Information, Southwest Minzu University, State Ethnic Affairs Commission, Chengdu 610041, China; Institute of Chemical Materials, China Academy of Engineering Physics, Mianyang 621900, China; Institute of Microelectronics and Nanoelectronics, College of Information Science and Electronic Engineering, Zhejiang University, Hangzhou 310007, China; Email: 80300024@swun.edu.cn

Yang Qiu - Pico center, SUSTech Core Research Facilities, Southern University of Science and Technology, Shenzhen 518055, China; Email: qiuy@sustech.edu.cn

Xudong Cui - Institute of Chemical Materials, China Academy of Engineering Physics, Mianyang 621900, China; Email: xudcui@caep.cn

Co-authors:

Yong Deng – College of Electronic and Information, Southwest Minzu University, State Ethnic Affairs Commission, Chengdu 610047, China; Pico center, SUSTech Core Research Facilities, Southern University of Science and Technology, Shenzhen 518055, China

Nan Xie - Institute of Integrated Circuits, China Center for Information Industry Development, Beijing 100048, China; State Key Laboratory of Artificial Microstructure and Mesoscopic Physics, School of Physics, Peking University, Beijing 100871, China

Wenyu Hu - Materials Characterization and Preparation Center and Department of Physics, Southern University of Science and Technology, Shenzhen 518056, China

Zhenyu Ma - Southwest Minzu University, State Ethnic Affairs Commission, Chengdu 610048, China

Fujun Xu - State Key Laboratory of Artificial Microstructure and Mesoscopic Physics, School of Physics, Peking University, Beijing 100871, China

Longqing Chen, Wenbin Qiu - Key laboratory of Radiation Physics and Technology of Ministry of Education, Institute of Nuclear Science and Technology, Sichuan University, Chengdu 610064, China

Lin Zhao, Hong Tao, Bo Wu, Yi Huang, Jian Ma, Xuqi Zhang - College of Electronic and Information, Southwest Minzu University, State Ethnic Affairs Commission, Chengdu 610046, China

Chaoyuan Jin - Institute of Microelectronics and Nanoelectronics, College of Information Science and Electronic Engineering, Zhejiang University, Hangzhou

310007, China; Zhejiang Laboratory, Hangzhou 311121, China; International Joint Innovation Center, Zhejiang University, Haining 314400, China

Marie-Pierre Chauvat, - CIMAP, UMR 6252, CNRS-ENSICAEN-CEA-UCBN, 6 Boulevard Maréchal Juin, 14050 Caen, Cedex 04, France

Pierre Ruterana - CIMAP, UMR 6252, CNRS-ENSICAEN-CEA-UCBN, 6 Boulevard Maréchal Juin, 14050 Caen, Cedex 04, France

Thomas Walther – Dept. Electronic & Electrical Eng., University of Sheffield, Mappin St., Sheffield S1 3JD, UK

Author Contributions

Yong Deng and Nan Xie contributed equally to this work. Xiaoyi Wang, Yang Qiu Xudong Cui and Thomas Walther conceived the research. Nan Xie and Fujun Xu conducted the growth of AlN thin film as well as the XRD and AFM measurements. Thomas Walther suggested and advised on the use of the STEM moiré technique. The scan rotation and atomic resolution images were acquired by Yong Deng and Wenyu Hu. Yong Deng, Zhenyu Ma and Xuqi Zhang analyzed the visible Moiré pattern based on atomic models. Marie-Pierre Chauvat prepared TEM samples using the FIB and did the weak beam investigation. Pierre Ruterana monitored the weak beam measurements and did the analysis. All the authors contributed to data processing, results discussion and manuscript writing.

Notes

The Authors declare no competing financial interest.

Acknowledgement

This research is supported by the Fundamental Research Fund for the Central Universities, Southwest Minzu University, China (2021NYYXS104); Technology and Innovation Commission of the Shenzhen Municipality (JCYJ20190809142019365); National Natural Science Foundation of China (12005151, 12005152); National Key Research and Development Program of China (2021YEB2800500); National Natural Science Foundation of China (61574138, 61905217, 61974131); Natural Science Foundation of Zhejiang Province (LGJ21F050001); Major Scientific Project of Zhejiang Laboratory (2019MB0AD01). The authors acknowledge the assistance of SUSTech Core Research Facilities and the help of Dr. DS He at Pico Center for the aberration corrected TEM experiments. Part of the TEM samples were prepared using a FIB facility, which was acquired through the EQUIPEX GENESIS ANR-11-EQPX-0020 within the French “Investissements d’avenir” national Programme with the contribution of the Region Normandie through the FEDER system. Conventional TEM analysis was carried in the CNRS Federation IRMA - FR 3095.

References

(1) Taniyasu, Y.; Kasu, M.; Makimoto, T. An Aluminium Nitride Light-Emitting Diode with a Wavelength of 210 Nanometres. *Nature* **2006**, *441* (7091), 325–328.

(2) Laleyan, D. A.; Zhao, S.; Woo, S. Y.; Tran, H. N.; Le, H. B.; Szkopek, T.; Guo, H.; Botton, G. A.; Mi, Z. AlN/h-BN Heterostructures for Mg Dopant-Free Deep Ultraviolet Photonics. *Nano Lett.* **2017**, *17* (6), 3738–3743.

(3) Zheng, W.; Huang, F.; Zheng, R.; Wu, H. Low-Dimensional Structure Vacuum-Ultraviolet-Sensitive ($\lambda < 200$ nm) Photodetector with Fast-Response Speed Based on High-Quality AlN Micro/Nanowire. *Adv. Mater.* **2015**, *27* (26), 3921–3927.

(4) Khan, A.; Balakrishnan, K.; Katona, T. Ultraviolet Light-Emitting Diodes Based on Group Three Nitrides. *Nat. Photonics* **2008**, *2* (2), 77–84.

(5) Growden, T. A.; Zhang, W.; Brown, E. R.; Storm, D. F.; Meyer, D. J.; Berger, P. R. Near-UV Electroluminescence in Unipolar-Doped, Bipolar-Tunneling GaN/AlN Heterostructures. *Light Sci. Appl.* **2018**, *7* (2), 17150–17150.

(6) Chen, Z.; Liu, Z.; Wei, T.; Yang, S.; Dou, Z.; Wang, Y.; Ci, H.; Chang, H.; Qi, Y.; Yan, J.; Wang, J.; Zhang, Y.; Gao, P.; Li, J.; Liu, Z. Improved Epitaxy of AlN Film for Deep-Ultraviolet Light-Emitting Diodes Enabled by Graphene. *Adv. Mater.* **2019**, *31* (23), 1807345.

(7) Lähnemann, J.; Den Hertog, M.; Hille, P.; de la Mata, M.; Fournier, T.; Schörmann, J.; Arbiol, J.; Eickhoff, M.; Monroy, E. UV Photosensing Characteristics of Nanowire-Based GaN/AlN Superlattices. *Nano Lett.* **2016**, *16* (5), 3260–3267.

(8) Zhou, S.; Zhao, X.; Du, P.; Zhang, Z.; Liu, X.; Liu, S.; Jay Guo, L. Application of Patterned Sapphire Substrate for III-Nitride Light-Emitting Diodes. *Nanoscale* **2022**, *14* (13), 4887–4907.

(9) Bai, J.; Dudley, M.; Sun, W. H.; Wang, H. M.; Khan, M. A. Reduction of Threading Dislocation Densities in AlN/sapphire Epilayers Driven by Growth Mode Modification. *Appl. Phys. Lett.* **2006**, *88* (5), 051903.

(10) Wu, Y.; Hanlon, A.; Kaeding, J. F.; Sharma, R.; Fini, P. T.; Nakamura, S.; Speck, J. S. Effect of Nitridation on Polarity, Microstructure, and Morphology of AlN Films. *Appl. Phys. Lett.* **2004**, *84* (6), 912–914.

(11) Sadeghi, B.; Cavaliere, P.; Balog, M.; Pruncu, C. I.; Shabani, A. Microstructure Dependent Dislocation Density Evolution in Micro-Macro Rolled Al_2O_3/Al Laminated Composite. *Mater. Sci. Eng. A* **2022**, *830*, 142317.

(12) Eng, P. J.; Trainor, T. P.; Brown Jr., G. E.; Waychunas, G. A.; Newville, M.; Sutton, S. R.; Rivers, M. L. Structure of the Hydrated α-Al_2O_3 (0001) Surface. *Science* **2000**, *288* (5468), 1029–1033.

(13) Northrup, J. E.; Di Felice, R.; Neugebauer, J. Atomic Structure and Stability of AlN (0001) and (000$\bar{1}$) Surfaces. *Phys. Rev. B* **1997**, *55* (20), 13878–13883.

(14) Meng, F.; Estruga, M.; Forticaux, A.; Morin, S. A.; Wu, Q.; Hu, Z.; Jin, S. Formation of Stacking Faults and the Screw Dislocation-Driven Growth: A Case Study of Aluminum Nitride Nanowires. *ACS Nano* **2013**, *7* (12), 11369–11378.

(15) Ruterana, P.; Barbaray, B.; Béré, A.; Vermaut, P.; Hairie, A.; Paumier, E.; Nouet, G.; Salvador, A.; Botchkarev, A.; Morkoç, H. Formation Mechanism and Relative Stability of the {11-20} Stacking Fault Atomic Configurations in Wurtzite (Al,Ga,In) Nitrides. *Phys. Rev. B* **1999**, *59* (24), 15917–15925.

(16) Bai, J.; Wang, T.; Parbrook, P. J.; Lee, K. B.; Cullis, A. G. A Study of Dislocations in AlN and GaN Films Grown on Sapphire Substrates. *J. Cryst. Growth* **2005**, *282* (3), 290–296.

(17) Liu, L.; Zhang, X.; Wang, S.; Wang, G.; Yu, J.; Hu, X.; Xu, Q.; Xu, X.; Zhang, L. Nucleation Mechanism of GaN Crystal Growth on Porous GaN/Sapphire Substrates. *CrystEngComm* **2022**, *24* (10), 1840–1848.

(18) Mouti, A.; Rouvière, J.-L.; Cantoni, M.; Carlin, J.-F.; Feltin, E.; Grandjean, N.; Stadelmann, P. Stress-Modulated Composition in the Vicinity of Dislocations in Nearly Lattice Matched $Al_xIn_{1-x}N$/GaN Heterostructures: A Possible Explanation of Defect Insensitivity. *Phys. Rev. B* **2011**, *83* (19), 195309.

(19) Miyake, H.; Nishio, G.; Suzuki, S.; Hiramatsu, K.; Fukuyama, H.; Kaur, J.; Kuwano, N. Annealing of an AlN Buffer Layer in N_2–CO for Growth of a High-Quality AlN Film on Sapphire. *Appl. Phys. Express* **2016**, *9* (2), 025501.

(20) Arulkumaran, S.; Sakai, M.; Egawa, T.; Ishikawa, H.; Jimbo, T.; Shibata, T.; Asai, K.; Sumiya, S.; Kuraoka, Y.; Tanaka, M.; Oda, O. Improved Dc Characteristics of AlGaN/GaN High-Electron-Mobility Transistors on AlN/Sapphire Templates. *Appl. Phys. Lett.* **2002**, *81* (6), 1131–1133.

(21) Tang, B.; Hu, H.; Wan, H.; Zhao, J.; Gong, L.; Lei, Y.; Zhao, Q.; Zhou, S. Growth of High-Quality AlN Films on Sapphire Substrate by Introducing Voids through Growth-Mode Modification. *Appl. Surf. Sci.* **2020**, *518*, 146218.

(22) He, C.; Zhao, W.; Wu, H.; Liu, N.; Zhang, S.; Li, J.; Jia, C.; Zhang, K.; He, L.; Chen, Z.; Shen, B. Fast Growth of Crack-Free Thick AlN Film on Sputtered AlN/Sapphire by Introducing High-Density Nano-Voids. *J. Phys. Appl. Phys.* **2020**, *53* (40), 405303.

(23) Zhang, K.; Wu, H.; Wang, Q.; Zhao, W.; Li, C.; Ren, Y.; Liu, N.; He, L.; He, C.; Chen, Z. Interfacial Engineering for Semi-Insulating GaN/Sapphire Template with Low Dislocation Density. *J. Alloys Compd.* **2022**, *901*, 163609.

(24) Xu, F. J.; Zhang, L. S.; Xie, N.; Wang, M. X.; Sun, Y. H.; Liu, B. Y.; Ge, W. K.; Wang, X. Q.; Shen, B. Realization of Low Dislocation Density AlN on a Small-Coalescence-Area Nano-Patterned Sapphire Substrate. *CrystEngComm* **2019**, *21* (15), 2490–2494.

(25) Tang, B.; Wan, Z.; Hu, H.; Gong, L.; Zhou, S. Strain Management and AlN Crystal Quality Improvement with an Alternating V/III Ratio AlN Superlattice. *Appl. Phys. Lett.* **2021**, *118* (26), 262101.

(26) Long, H.; Dai, J.; Zhang, Y.; Wang, S.; Tan, B.; Zhang, S.; Xu, L.; Shan, M.; Feng, Z. C.; Kuo, H.; Chen, C. High Quality 10.6 μm AlN Grown on Pyramidal Patterned Sapphire Substrate by MOCVD. *Appl. Phys. Lett.* **2019**, *114* (4), 042101.

(27) Liu, B.; Xu, F.; Wang, J.; Lang, J.; Zhang, N.; Fang, X.; Wang, L.; Yang, X.; Kang, X.; Wang, X.; Qin, Z.; Ge, W.; Shen, B. High Quality AlN with Uniform In-Plane Strain on Nano-Patterned AlN Templates Achieved by Preset Strain Modulation. *Jpn. J. Appl. Phys.* **2021**, *60* (12), 120903.

(28) Zhao, Y.; Yang, Y.; Wen, H.; Liu, C.; Huang, X.; Liu, Z. Evaluation of Interfacial Misfit Strain Field of Heterostructures Using STEM Nano Secondary Moiré Method. *Phys. Chem. Chem. Phys.* **2022**, *24* (17), 9848–9854.

(29) Pofelski, A.; Ghanad-Tavakoli, S.; Thompson, D. A.; Botton, G. A. Sampling Optimization of Moiré Geometrical Phase Analysis for Strain Characterization in Scanning Transmission Electron Microscopy. *Ultramicroscopy* **2020**, *209*, 112858.

(30) Pofelski, A.; Woo, S. Y.; Le, B. H.; Liu, X.; Zhao, S.; Mi, Z.; Löffler, S.; Botton, G. A. 2D Strain Mapping Using Scanning Transmission Electron Microscopy Moiré Interferometry and Geometrical Phase Analysis. *Ultramicroscopy* **2018**, *187*, 1–12.

(31) Kondo, Y.; Aoyama, Y.; Hashiguchi, H.; Lin, C. C.; Hsu, K.; Endo, N.; Asayama, K.; Fukunaga, K.-I. Strain Measurement of a Channel between Si/Ge Stressors in a Tri-Gate Field Effect Transistor Utilizing Moiré Fringes in Scanning Transmission Microscope Images. *Appl. Phys. Lett.* **2019**, *114* (17), 172103.

(32) Su, D.; Zhu, Y. Scanning Moiré Fringe Imaging by Scanning Transmission Electron Microscopy. *Ultramicroscopy* **2010**, *110* (3), 229–233.

(33) Lin, Y.-C.; Ji, H. G.; Chang, L.-J.; Chang, Y.-P.; Liu, Z.; Lee, G.-D.; Chiu, P.-W.; Ago, H.; Suenaga, K. Scanning Moiré Fringe Method: A Superior Approach to Perceive Defects, Interfaces, and Distortion in 2D Materials. *ACS Nano* **2020**, *14* (5), 6034–6042.

(34) Xie, N.; Xu, F.; Zhang, N.; Lang, J.; Wang, J.; Wang, M.; Sun, Y.; Liu, B.; Ge, W.; Qin, Z.; Kang, X.; Yang, X.; Wang, X.; Shen, B. Period Size Effect Induced Crystalline Quality Improvement of AlN on a Nano-Patterned Sapphire Substrate. *Jpn. J. Appl. Phys.* **2019**, *58* (10), 100912.

(35) Béré, A.; Ruterana, P.; Chauvat, M.-P.; Koulidiati, J. Atomic Core Structures Associated to the Threading Dislocation with $<1\bar{1}00>$ Burgers Vector and [0001] Line Direction in GaN. *Jpn. J. Appl. Phys.* **2013**, *52* (11S), 11NG06.

(36) Ruterana, P.; Morales, M.; Chery, N.; Ngo, T. H.; Chauvat, M.-P.; Lekhal, K.; Damilano, B.; Gil, B. Effect of AlGaN Interlayer on the GaN/InGaN/GaN/AlGaN Multi-Quantum Wells Structural Properties toward Red Light Emission. *J. Appl. Phys.* **2020**, *128* (22), 223102.

(37) Williams, D. B.; Carter, C. B. Phase-Contrast Images. In *Transmission Electron Microscopy: A Textbook for Materials Science*; Williams, D. B., Carter, C. B., Eds.; Springer US: Boston, MA, 2009; pp 389–405.

(38) Jiang, K.; Sun, X.; Ben, J.; Jia, Y.; Liu, H.; Wang, Y.; Wu, Y.; Kai, C.; Li, D. The Defect Evolution in Homoepitaxial AlN Layers Grown by High-Temperature Metal–Organic Chemical Vapor Deposition. *CrystEngComm* **2018**, *20* (19), 2720–2728.

(39) Conesa-Boj, S.; Boioli, F.; Russo-Averchi, E.; Dunand, S.; Heiss, M.; Rüffer, D.; Wyrsch, N.; Ballif, C.; Miglio, L.; Morral, A. F. i. Plastic and Elastic Strain Fields in GaAs/Si Core–Shell Nanowires. *Nano Lett.* **2014**, *14* (4), 1859–1864.

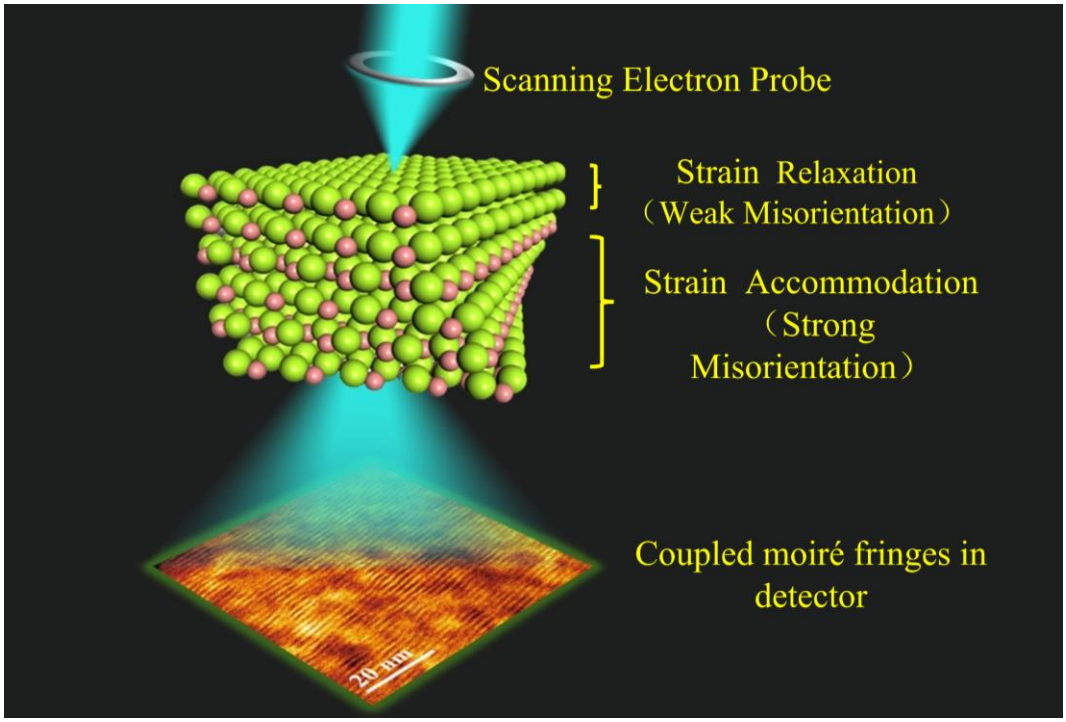

Table Of Contents graphic